◆ Human Brain Mapping 31:1327–1338 (2010) ◆

Correlation Between Quantitative EEG and MRI in Idiopathic Generalized Epilepsy

Luiz E. Betting,[1] Li M. Li,[1] Iscia Lopes-Cendes,[2] Marilisa M. Guerreiro,[1] Carlos A.M. Guerreiro,[1] and Fernando Cendes[1]*

[1]*Department of Neurology, Faculty of Medical Sciences, University of Campinas—UNICAMP, Campinas, SP, Brazil*
[2]*Department of Medical Genetics, Faculty of Medical Sciences, University of Campinas—UNICAMP, Campinas, SP, Brazil*

Abstract: The objective of this study was to investigate the relationship between the focal discharges sometimes observed in the electroencephalogram of patients with idiopathic generalized epilepsies and subtle structural magnetic resonance imaging abnormalities. The main hypothesis to be assessed is that focal discharges may arise from areas of structural abnormality which can be detected by quantitative neuroimaging. Focal discharges were used for quantitative electroencephalogram source detection. Neuroimaging investigations consisted of voxel-based morphometry and region of interest volumetry. For voxel-based morphometry, volumetric MRI were acquired and processed. The images of each patient were individually compared with a control group. Statistical analysis was used to detect differences in gray matter volumes. Region of interest-based morphometry was automatically performed and used essentially to confirm voxel-based morphometry findings. The localization of the focal discharges on the electroencephalogram was compared to the neuroimaging results. Twenty-two patients with idiopathic generalized epilepsies were evaluated. Gray matter abnormalities were detected by voxel-based morphometry analysis in 77% of the patients. There was a good concordance between EEG source detection and voxel-based morphometry. On average, the nearest voxels detected by these methods were 19 mm (mm) apart and the most statistically significant voxels were 34 mm apart. This study suggests that in some cases subtle gray matter abnormalities are associated with focal epileptiform discharges observed in the electroencephalograms of patients with idiopathic generalized epilepsies. *Hum Brain Mapp 31:1327–1338, 2010.*

Key words: epilepsy; neuroimaging; EEG source imaging; idiopathic generalized epilepsy; magnetic resonance

INTRODUCTION

Idiopathic generalized epilepsies (IGEs) are a group of epilepsies characterized by seizures with generalized onset [Commission on Classification and Terminology of the International League Against Epilepsy, ILAE, 1989]. An inter-ictal electroencephalogram (EEG) with typical generalized spike and wave (GSW) discharges and a normal background is supportive of IGE diagnosis [Panayiotopoulos, 2002]. Despite the criteria for diagnoses, focalities are not rare in the interictal EEG records of patients with IGE and several hypotheses have been proposed to explain their presence [Lombroso, 1997; Panayiotopoulos, 2002;

Additional Supporting Information may be found in the online version of this article.

Contract grant sponsor: Fundação de Amparo à Pesquisa do Estado de São Paulo (FAPESP).

*Correspondence to: Fernando Cendes, MD, PhD, Department of Neurology, Faculty of Medical Sciences, PO Box 6111, University of Campinas—UNICAMP, 13083-970, Campinas, SP, Brazil.
E-mail: fcendes@unicamp.br

Received for publication 22 February 2009; Revised 6 October 2009; Accepted 7 October 2009

DOI: 10.1002/hbm.20944

Published online 15 January 2010 in Wiley Online Library (wileyonlinelibrary.com).

Waltz, 2000]. Focalities may represent fragmented generalized discharges or focal cortical pathology, or they may represent localized self-sustaining hyperexcitability or be incidental findings [Lombroso, 1997]. The underlying etiology of focal discharges is currently under debate.

The pathophysiology of the GSW discharges involves an extensive network and mainly the thalamo-cortical circuitry. Challenging the assumption of diffuse cortical hyperexcitability related to the onset of the generalized seizures, experimental studies have suggested that these seizures have a focal background [Gloor, 1968; Meeren et al., 2002]. Therefore, defining the etiology of the EEG focalities observed in patients with IGE will provide an understanding of the mechanisms of these disorders and may confirm whether generalized seizures have a focal component.

Previous investigations using quantitative magnetic resonance imaging (MRI) detected subtle structural abnormalities in patients with IGE [Betting et al., 2006a; Woermann et al., 1999]. The combination of different imaging techniques may improve the detection of epileptogenic lesions and allow more precise assessment of neuronal function [Koepp and Woermann, 2005]. The objective of this study was to determine the relationship between focal EEG discharges and subtle structural MRI abnormalities in patients with IGE. The main hypothesis to be investigated is that focal discharges may arise from areas of structural abnormality which can be detected by multimodal quantitative neuroimaging.

METHODS

Subjects

Based on the presence of focalities in the EEG, 22 (12 women, mean age 30 ± 11 years, range 9–60) subjects were consecutively selected from 216 patients evaluated with IGE diagnosis. Patients were classified in three groups: juvenile myoclonic epilepsy (JME), epilepsy with generalized tonic-clonic seizures on awakening (GTCS) and absence epilepsy (AE) which included childhood absence epilepsy (CAE) and juvenile absence epilepsy. Patients classification was performed according to clinical and EEG criteria [ILAE, 1989; Panayiotopoulos, 2002]. All patients and one individual who had witnessed a typical seizure were reinterviewed, and the medical records were analyzed.

EEG Recording Protocol

All EEGs were performed in the interictal state. A 32-channel Nihon-Kohden EEG recorder was used with a digitization rate of 200 Hz. The ground electrode was placed at Fpz, and the band pass was situated at 0.3–70 Hz. In addition to the traditional 19 electrodes used in the international 10–20 system for electrode placement, two zigomatic fronto-temporal electrodes were also included for finer coverage of the temporal regions. The recording was made according to previous recommendations and included 20-min extent, hyperventilation and photic stimulation. At least one EEG record from each patient had the typical GSW discharges with normal background. The patients included in the study also had a minimum of one record with a clear focal or generalized asymmetrical epileptiform discharge. For this study, slow waves were not classified as focalities.

EEG Processing

EEG focalities or asymmetries were visually selected and stored using Neurofax software (EEG-1000, Version 04-01, Nihon-Kohden Corporation, Tokyo, Japan). Segments with artifacts were rejected from the analysis. The final preparation aligned the EEG segments, centered at the peak of the focal discharge with the higher amplitude, which was observed in the referential montage (with average). The segments were stored as two seconds durations (400 sample points). For the patients with more than one focal discharge, the selected segments were averaged. If a patient presented discharges in different locations, these focalities were individually analyzed.

EEG Source Detection

For localization, the Standardized Low Resolution Brain Electromagnetic Tomography (sLORETA) software was used [Pascual-Marqui, 2002]. This evaluation was performed for patients who had abnormalities detected during quantitative MRI analysis. Raw time-domain current density distributions were acquired for all of the individual two seconds epochs (time frames −1,000 to +1,000 ms). Such raw sLORETA values represent the power (the squared magnitude of the computed intracerebral current density) within 6,430 voxels at a 5-mm spatial resolution [Pascual-Marqui, 2002]. The grid in use is based on the digitized Talairach atlas [Talairach and Tournoux, 1988]. For source localization, sLORETA solutions were calculated for the average ascending phase (20 ms) of the focal discharge of interest. Previous investigations demonstrated that modeling in the ascending phase of the spike produce more reliable source identification [Huppertz et al., 2001; Scherg et al., 1999]. Region of interest (ROI) analysis was also conducted using the built-in sLORETA routines. There were 42 ROIs based on the Brodmann's areas (BAs) that were selected for each cerebral hemisphere. These ROIs were composed of a single centroid voxel located close to the center of each BA mass.

MRI Acquisition Protocol

Volumetric (3D) T1-weighted images with 1 mm isotropic voxels were acquired in a 2T (GE Elscint, Haifa, Israel) scanner using a spoiled gradient echo sequence

with flip angle = 35°, repetition time (TR) = 22 ms, echo time (TE) = 9 ms, matrix = 256 × 220, field of view (FOV) = 23 × 25 cm and 1-mm thick sagittal slices. This sequence was used for VBM analysis.

Image Processing

The images were acquired in the Digital Imaging and Communications in Medicine (DICOM) format. MRIcro software was used to transform the images into the ANALYZE format for the next steps [Rorden and Brett, 2000]. SPM5 software (Wellcome Trust Centre for Neuroimaging, London, England; available at: www.fil.ion.ucl.ac.uk) and VBM5 toolbox (available at: http://dbm.neuro.uni-jena.de) were used for image processing and statistical analysis. VBM5 toolbox employs a new unified segmentation approach which integrates image registration, MRI inhomogeneity bias correction and tissue classification [Ashburner and Friston, 2005; Meisenzahl et al., 2008]. All images underwent spatial normalization. Normalization reduces the interindividual variation due to brain size and positioning. Normalization was performed registering each image to the template of the International Consortium for Brain Mapping (Montreal Neurological Institute, Montreal, Canada). First, a 12-parameter affine transformation was used. Images were modulated in order to preserve tissue that was eventually deformed by the normalization protocol. Finally, the images were warped using nonlinear spatial transformations. Normalized images were corrected for non-uniformities in signal intensities and then submitted to automatic segmentation of the cerebrospinal fluid, white and gray matter, without the use of tissue priors. This approach reduces the population-specific bias and increases tissue classification accuracy. By applying a Hidden Markov Field model on segmented maps, VBM5 toolbox extends the unified segmentation approach and improves the quality of segmentation [Meisenzahl et al., 2008]. The algorithm used removes voxels that were isolated and are unlikely to be a member of a certain tissue class and close holes present in clusters of connected voxels resulting in a higher signal-to-noise ratio of the tissue probability maps [Meisenzahl et al., 2008]. For the present investigation, gray matter maps were used for VBM analysis. The final processing step consisted in smoothing the images convolving them with an 8-mm full-width at half maximum isotropic Gaussian kernel to reduce interindividual gyral variation.

MRI ROI Analysis

A ROI-based morphometric analysis was also conducted to strengthen the relationship between the EEG quantitative source analysis and the neuroimaging investigations. The Individual Brain Atlases using Statistical Parametric Mapping Software (IBASPM) toolbox was used to extract the volumes of 42 brain structures in each hemisphere. [Aléman-Gómez et al., 2006]. For this evaluation, we used an atlas of 84 segmented structures included in the IBASPM software. The volumes in cm^3 obtained for each individual were normalized based on the total intracranial volume of the controls. Next, the volumes were standardized relative to the volumes of normal controls subjects using a *Z*-score transformation.

VBM Statistical Analysis

The MRI images from each patient were individually compared to a control group of 20 healthy volunteers (10 women, mean age 31 ± 8, range 22–52). Each subject in the control group was also individually compared with the remaining 19 using analysis of variance and no gray matter abnormalities were detected. All patients and controls signed informed consent forms for participation. The study was approved by the local ethics committee. A voxel-by-voxel analysis of covariance (AnCova) was used to test for differences between the gray matter volumes of each patient and the control group. Age and gender were entered as covariates in the statistical design. The analysis included global grand mean scaling and proportional threshold masking of 0.4. The significance threshold selected was $P < 0.05$ corrected for multiple comparisons (false discovery rate).

EEG and VBM Distance Analysis

The Euclidian distances between the nearest voxel with the highest current density from the nearest suprathreshold voxel and the distance of the voxel with the highest current density from the most statistically significant voxel (nearest local maxima) were calculated. A 3D render of the brain overlaid with a graphical representation of the region with highest current density detected by sLORETA and the clusters of VBM statistically significant voxels was constructed to assist in the interpretation of the distance between the methods.

RESULTS

Clinical Features

Seven patients had JME (five women, mean age 26 ± 10 years, range 15–46). One of these patients presented myoclonic, absence and generalized tonic-clonic seizures, five presented myoclonic and generalized tonic-clonic seizures, and one presented myoclonic seizures only. Focal semiology suggestive of auras or partial complex seizures was described in four (57%) patients (Table I).

Eleven patients had AE (four women, mean age 22 ± 13 years, range 9–60). Two of these patients presented myoclonic, absence and generalized tonic-clonic seizures, seven

TABLE I. Clinical features of 22 IGE patients grouped by subsyndrome classification

Pat	Family history	Age[a]	Onset[a] sz	Last[a] sz	Gender	Seizure type	AED	Syndrome
3	Mother, brother, nephew	46	46	0	W	M, G	CBZ	JME
7	Negative	33	23	10	M	M, G	VPA	JME
8	Four cousins	29	13	1	W	M, A, G	VPA	JME
15	Father, sister	18	7	2	M	M, G	VPA	JME
16	Mother, grandfather and uncle	15	14	0	W	M	VPA	JME
19	Uncle, sister	22	22	0	W	M, G	None	JME
22	Sister	23	9	1	W	M, G	CBZ	JME
4	Negative	31	18	0	M	A, G	VPA	JAE
5	Uncle	21	14	1	M	A, G	VPA	JAE
6	Uncle, ant, cousin	22	11	0	M	A, G	LMT	JAE
10	Grandfather, uncle	10	8	1	W	A, G	VPA	CAE
11	Negative	60	29	1	M	M, A, G	VPA	JAE
12	Negative	20	13	0	M	A	VPA	JAE
13	Negative	16	10	2	M	A, G	VPA	JAE
14	Grandmother	9	2	0	W	A	ETX	CAE
17	Uncle, grandmother	22	4	1	W	M, A, G	VPA	JAE
18	Sister	18	6	0	M	A, G	VPA	JAE
21	Two uncles	19	16	2	W	A, G	VPA	JAE
1	Father, sister	35	11	1	M	G	CBZ	GTCS
2	Negative	29	15	1	W	G	CBZ	GTCS
9	Uncle	19	7	1	W	M, G	CBZ	GTCS
20	Two sisters, ant, nephews	32	13	2	W	G	DPH	GTCS

The MRI VBM analyses of patients 3, 7, 9, 13 and 15 presented no abnormalities when individually compared with the controls.
Family history, family members with epilepsy; Pat, patient; M, man; W, woman; M, myoclonic; A, absence; G, generalized tonic-clonic seizures; AED, antiepileptic drug; VPA, valproate; CBZ, carbamazepine; DPH, phenytoin; ETX, ethossuximide; JME, juvenile myoclonic epilepsy; CAE, childhood absence epilepsy; JAE, juvenile absence epilepsy; GTCS, generalized tonic-clonic seizures on awakening; sz, seizure.
[a]Expressed in years.

presented absence and generalized tonic-clonic seizures, and two presented absence seizures only. Focal semiology suggestive of auras or partial complex seizures was described in two (18%) patients (Table I).

Four patients had GTCS (three women, mean age 28 ± 7 years, range 19–35). One patient presented myoclonic and generalized tonic-clonic seizures, and three presented generalized tonic-clonic seizures only. Focal semiology suggestive of auras or partial complex seizures was not described in any of the GTCS patients (Table I).

Head injury and other risk factors for epilepsy were investigated. Only two patients have a positive history for head injury. One of these had a skull fracture at 7 years with no neurological complications. The other patient described a minor trauma with temporary loss of conscience. In both patients, there was no evidence of lesion in the visual analysis of the MRI.

EEG Features

Ninety-three EEG records were reevaluated. A mean of 4 ± 2 EEG recordings were performed on each patient (range 1–9). There were 26 EEG exams performed in the JME group, and 12 (46%) showed focalities. The persistence of focalities ranged from 8 months to 5 years. In three patients, focalities were present in only one record. Two patients presented different focality patterns in their EEG profiles. There were 43 EEG exams performed in the AE group, and 17 (39%) showed focalities. The persistence of focalities ranged from 1 month to 4 years. In seven patients, focalities were present in only one record. Three patients presented different focality patterns in their EEG profiles. There were 24 EEG exams performed in the GTCS group, and 11 (45%) showed focalities. The persistence of focalities ranged from 1 month to 9 years. In one patient, focalities were present in only one record. One patient presented different focality patterns in their EEG profiles. Table II summarizes these findings.

EEG Source Detection

In total, 117 focal discharges of 17 patients were evaluated (mean 5 ± 9, range 1–46). Four patients had only a single epileptiform discharge available for source analysis. Six patients had discharges in different locations. Source analysis was performed in 23 processed discharges. Table III shows the areas of current density maxima with the respective coordinates. Figures 1 and 2 and Supporting Information, Figures 1–3 show the discharges evaluated (Parts A and C) and an example of the generalized discharge (Part

TABLE II. General EEG features observed in 22 IGE patients

	JME	AE	GTCS	Total
Total of EEGs performed (*n*)	26	43	24	93
Focalities	12 (46%)	17 (39%)	11 (45%)	40 (43%)
Persistence of location[a]	3 patients	4 patients	3 patients	10 patients

JME, juvenile myoclonic epilepsy; AE, absence epilepsy; GTCS, generalized tonic-clonic seizures on awakening.
[a]Defined as the presence of a focality detected in the same location in two distinct EEG records, regardless of the time interval between records.

B). The sLORETA source solutions were overlaid with a T1 MRI anatomical template and with 3D render (Figs. 1 and 2 and Supporting Information, Figs. 1–3, Part E, superior and middle panels, respectively). Part D of the figures shows the results of the EEG ROI analysis. A spatiotemporal map of the current density was constructed based on the raw current density values of timeframes 150–300 [Zumsteg et al., 2006]. The current values were color-coded to facilitate visualization, and the arrows indicate the local of current maxima obtained using the average technique [Zumsteg et al., 2006].

MRI and Voxel-Based Morphometry (VBM) Analysis

All MRI images were visual analyzed, and no significant abnormalities were observed. The VBM comparisons showed areas of gray matter abnormalities in 17 of the 22 (77%) patients evaluated. Fifteen of the 17 (88%) patients showed areas of increased gray matter volumes. The other two (12%) patients showed a mixed pattern of atrophy and increased gray matter volume.

Juvenile myoclonic epilepsy

Four of the seven (57%) patients had areas of abnormal gray matter. The areas of abnormal gray matter were located in the right rectal, inferior, middle and medial frontal gyrus and in the left postcentral gyrus, parietal and occipital lobe (posterior portion of the middle temporal gyrus).

Absence epilepsy

Ten of the 11 (91%) patients had areas of abnormal gray matter. The areas of abnormal gray matter were located in the right superior, medial, middle and inferior frontal gyrus, postcentral gyrus, fusiform gyrus, cingulated gyrus and parietal lobe and in the left parietal lobe, middle and medial frontal gyrus, middle and superior temporal gyrus.

Generalized tonic-clonic seizures

Three of four (75%) patients had areas of abnormal gray matter. The areas of abnormal gray matter volume were located at the left inferior frontal gyrus, right insula and right parietal lobe.

Table III shows the areas of gray matter abnormalities, which were detected by the VBM analysis, with their respective coordinates. Figures 1 and 2 and Supporting Information, Figures 1–3 (Part E, inferior panel) displays these areas overlaid with an anatomical T1 MRI template.

ROI Volumetry Analysis

In 12 of the 17 (70%) patients the ROI volumetry analysis showed analogous results to the EEG source detection and VBM (patients 2, 4, 6, 8, 10, 12, 14, 16, 19, 20, 21 and 22). In seven of the 17 patients (41%), the thalamic volumes were abnormal. Atrophy was observed in three patients (bilateral in two), and increased thalamic volumes were observed in four patients (unilateral). Figure 3 and Supporting Information, Figure 4 show the results of the measured volumes. Standardized volumes and details about segmented structures are provided in Supporting Information, Table I.

EEG and VBM Distance Analysis

The mean distance of the nearest voxel with the highest current density detected by sLORETA from the VBM nearest suprathreshold voxel was 19 ± 20 mm (range 1–98) for all the evaluated processed discharges, 17 ± 14 (1–38) for JME patients, 20 ± 22 (5–98) for AE patients and 23 ± 19 (6–44) for GTCS patients. The mean distance between the voxel with the highest current density detected by sLORETA from the most statistically significant voxel (nearest local maxima) detected by VBM was 34 ± 17 (12–98) for all the evaluated processed discharges, 31 ± 9 (17–38) for JME patients, 36 ± 19 (14–98) for AE patients and 33 ± 24 (12–59) for GTCS patients. The individual distances are described in Table III. Figure 4 and Supporting Information, Figure 5 show the voxels with highest current density detected by sLORETA and the clusters of VBM statistically significant voxels in a 3D brain model.

DISCUSSION

The present work yielded two major findings. The first major finding is that 77% of patients with IGE and EEG

TABLE III. Results of EEG source analysis and voxel-based morphometry of 17 patients with IGE

	EEG/sLORETA					MRI/VBM							
P#	*X*	*Y*	*Z*[a]	Localization	Value[b]	*X*	*Y*	*Z*	Localization	*P*-value	Cluster	*D*	
8	−65	−55	15	Superior temporal gyrus	0.81	−69	−19	25	Postcentral gyrus	0.03	3860	38	*A/B*
16	−35	−85	30	Occipital lobe	0.07	−33	−63	19	Occipital lobe	0.001	1252	25	*A*
	−35	−80	40	Parietal lobe	0.07	−32	−61	11	Occipital lobe			35	*B*
19	10	20	−30	Rectal gyrus	0.57	9	9	−26	Rectal gyrus	0.006	628	11	*A*
	−60	−65	5	Middle temporal gyrus	0.21	−59	−65	5	Middle temporal gyrus	0.03	10852	1	*A*
	10	20	−30	Rectal gyrus	0.57	9	5	−23	Medial frontal gyrus			17	*B*
	−40	−85	30	Occipital gyrus	0.21	−42	−64	48	Parietal lobe			28	*B*
22	30	40	−5	Middle frontal gyrus	0.35	30	42	6	Middle frontal gyrus	0.007	181	12	*A*
	25	35	−5	Inferior frontal gyrus	0.36	28	7	19	Inferior frontal gyrus			37	*B*
4[c]	40	50	−15	Middle frontal gyrus	0.12	24	50	−10	Middle frontal gyrus	<0.001	6132	17	*A*
	−35	55	−10	Middle frontal gyrus	0.23	−27	55	−10	Middle frontal gyrus	0.01	6574	9	*A*
	50	45	−10	Inferior frontal gyrus	0.13	18	49	−11	Middle frontal gyrus			32	*B*
	−40	55	−10	Middle frontal gyrus	0.23	−51	33	2	Middle frontal gyrus			27	*B*
5	35	40	−10	Middle frontal gyrus	0.87	28	40	−2	Middle frontal gyrus	0.001	1061	11	*A*
	−30	40	−15	Middle frontal gyrus	3.0	−32	44	−7	Middle frontal gyrus	0.001	434	9	*A*
	35	40	−10	Middle frontal gyrus	0.87	27	34	14	Inferior frontal gyrus			26	*B*
	−30	35	−15	Middle frontal gyrus	3.0	−38	−3	−25	Middle frontal gyrus			40	*B*
6	25	40	−10	Middle frontal gyrus	2.2	30	38	14	Middle frontal gyrus	0.002	294	25	*A*
	−35	20	−25	Superior temporal gyrus	0.06	−37	−2	−21	Superior temporal gyrus	0.002	1113	23	*A*
	15	45	−25	Orbital gyrus	1.2	27	34	14	Medial frontal gyrus			42	*B*
	−20	35	−25	Orbital gyrus	0.59	−38	−3	−25	Middle temporal gyrus			42	*B*
10	40	−30	20	Insula	0.42	43	−23	29	Postcentral gyrus	<0.001	5336	12	*A*
	60	−5	−30	Fusiform gyrus	0.50	53	−40	−35	fusiform gyrus			36	*B*
11	25	55	−15	Superior frontal gyrus	0.98	20	53	−13	superior frontal gyrus	0.001	332	5	*A*
	−35	45	15	Middle frontal gyrus	0.73	−18	45	4	Medial frontal gyrus	<0.001	4235	20	*A*
	30	55	−15	Superior frontal gyrus	0.99	18	49	−12	Superior frontal gyrus			14	*B*
	−35	50	30	Superior frontal gyrus	0.84	−26	14	32	Middle frontal gyrus			37	*B*
12	−35	55	−10	Middle frontal gyrus	0.97	−39	41	−13	Middle frontal gyrus	0.03	187	14	*A*
	−25	60	−15	Superior frontal gyrus	0.99	−41	38	−14	Middle frontal gyrus			27	*B*
14	45	−25	55	Parietal lobe	0.73	33	−32	62	Parietal lobe	0.04	842	15	*A*
	−55	−40	35	Parietal lobe	2.4	−40	−44	30	Parietal lobe	0.01	650	16	*A*
	60	−25	50	Postcentral gyrus	0.76	25	−27	42	Cingulated gyrus			36	*B*
	−50	−35	60	Parietal lobe	2.5	−33	−25	30	Parietal lobe			36	*B*
17	25	55	−5	Middle frontal gyrus	0.26	24	41	−5	Middle frontal gyrus	<0.001	3373	14	*A*
	25	65	−5	Superior frontal gyrus	0.27	22	41	−3	Middle frontal gyrus			24	*B*
18	45	45	−15	Middle frontal gyrus	0.44	36	−48	13	Postcentral gyrus	0.01	1925	98	*A/B*
21	−5	20	−20	Medial frontal gyrus	0.15	0	20	−12	Medial frontal gyrus	<0.001	37535	9	*A*
	−5	25	−25	Rectal gyrus	0.16	−11	6	−22	Medial frontal gyrus			20	*B*
1	−30	10	−20	Inferior frontal gyrus	0.87	−37	27	−14	Inferior frontal gyrus	0.02	524	20	*A*
	−35	5	−20	Superior temporal gyrus	0.89	−40	31	−12	Inferior frontal gyrus			28	*B*
2	45	35	20	Middle frontal gyrus	0.24	26	−4	18	Insula	0.002	1967	44	*A*
	50	40	20	Middle frontal gyrus	0.26	20	−8	5	Insula			59	*B*
20	30	−50	65	Superior parietal lobule	0.04	28	−48	59	Superior parietal lobule	0.006	157	6	*A*
	35	−45	65	Postcentral gyrus	0.04	28	−49	56	Parietal lobe			12	*B*

Patients are listed according to subsyndrome classification described in Table I. The distances between the nearest voxel with the highest current density from the VBM nearest suprathreshold voxel (*A*) and the distance of the voxel with the highest current density from the most statistically significant voxel (*B*, nearest local maxima) detected by VBM are depicted. VBM analysis was performed by searching for gray matter concentration abnormalities. The statistical level of significance was $P < 0.05$ corrected for multiple comparisons (false discovery rate).

P#, patient number; D, euclidian distance between the sLORETA and VBM voxel (mm).

[a]*X*, *Y* and *Z* represent Montreal Neurological Institute coordinates expressed in millimeters (mm).

[b]Current density value in miliamperes/mm^2.

[c]Patients with a mixed pattern of atrophy and increased gray matter volume.

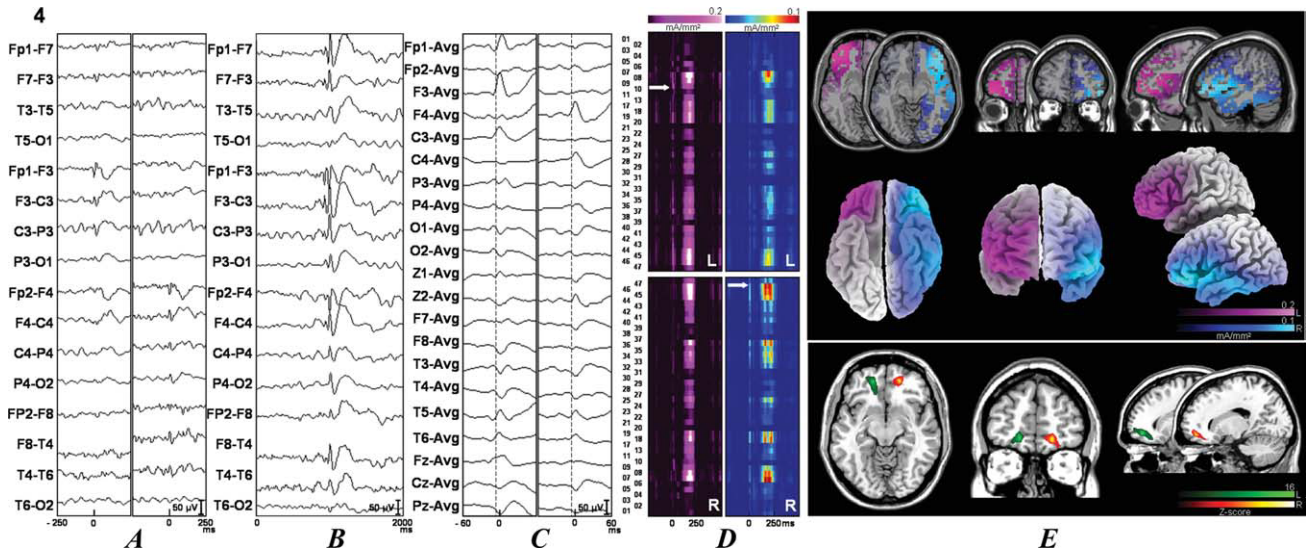

Figure 1.

Two EEG samples and source analysis and individual VBM comparisons of IGE patients with 20 controls searching for gray matter abnormalities. The data for patients 4 (see Fig. 1) and 14 (see Fig. 2) are shown. See Suplementary Figures 1–3 for results from the rest of the patients. The patient number is indicated at the upper left portion of the figure. (**A**) Examples of focal discharges. When two different discharges were present, they were independently illustrated. The left column corresponds to the left discharge, and the right column corresponds to the right discharge. (**B**) Examples of the generalized discharges. (**C**) Discharges submitted to source analyses with sLORETA in a different time window. (**D**) sLORETA solutions map showing the current densities according to their Brodmann's areas. (**E**) sLORETA solutions in a anatomical template (superior panel) and in a 3D rendering (middle panel). When there were two different discharges, the left discharge is depicted in the pink scale, and the right discharge is depicted in the jet or cold scale in (D) and (E). The inferior panel shows the VBM analysis results. The VBM results (colored areas) are superimposed on an anatomical template. The colors represent the number of standard deviations compared with the controls, as indicated by the scale in the right inferior portion of the figure. Green scale was used for abnormalities in the left (L) hemisphere and hot scale for abnormalities in the right (R) hemisphere. Patient 4 (see Fig. 1) had predominantly areas of atrophy and patient 14 (see Fig. 2) had areas of increased gray matter volumes. Statistical analysis was performed with a corrected $P < 0.05$ (false discovery rate). Figures are depicted in the neurological convention (right on right).

focalities have an area of subtle structural abnormality, which can be detected by VBM analysis. Secondly, we observed a good concordance between the source analysis of the EEG focalities and the MRI gray matter abnormalities which were detected by VBM. Therefore, our study suggests that anomalous gray matter volumes present in the brains of some IGE patients are related with the focal interictal epileptiform discharges observed in their EEGs. This observation is strong evidence which supports the postulated hypothesis that in some patients with IGE, focal EEG discharges may arise from subtle structural abnormalities.

sLORETA was validated as a reliable method for source localization [Grova et al., 2006; Zumsteg et al., 2006]. The average technique we used may sometimes falsely localize the epileptic source, especially when located in deep structures [Zumsteg et al., 2006]. The reduced number of electrodes and the sampling rate also may influence the EEG source detection. Furthermore, in the present investigation, only routine EEGs were evaluated and in four cases only one discharge was available for source analysis. In these situations, the noise level may be elevated reducing localization accuracy. Nevertheless, there was a good concordance between the methods with an average of 20 mm for the nearest voxels and 34 mm for the voxels with maximum values. The best correlation between neuroimaging and EEG studies was 10–16 mm described in evoked potentials experiments [Grova et al., 2008]. In the evaluation of the generators of interictal spikes, previous investigations using EEG-fMRI and EEG source localization showed a distance greater than 30 mm between the methods [Bagshaw et al., 2006]. Moreover, evaluating the distance between the nearest voxel with the highest current density and VBM nearest suprathreshold voxel, 78% (18 of 23) of the processed discharges were in the same anatomical structure and 74% (17 of 23) had a distance inferior than 20 mm which is in the range of the sLORETA resolution that is presumed to be between 10 and 20 mm [Mulert et al., 2004].

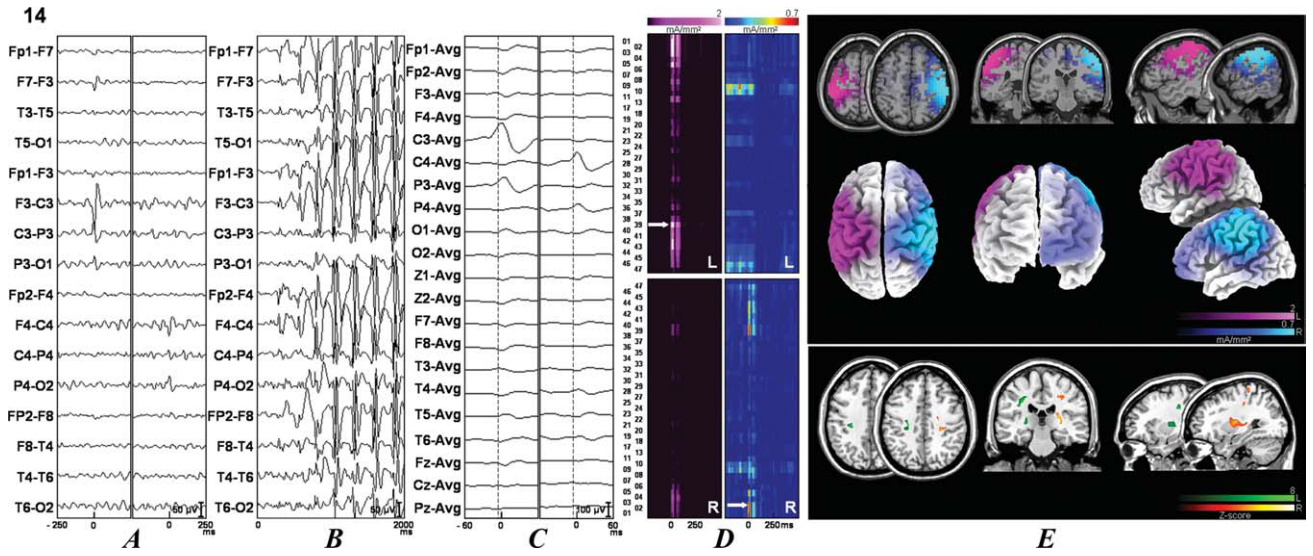

Figure 2.

Two EEG samples and source analysis and individual VBM comparisons of IGE patients with 20 controls searching for gray matter abnormalities. The data for patients 4 (see Fig. 1) and 14 (see Fig. 2) are shown. See Suplementary Figures 1–3 for results from the rest of the patients. The patient number is indicated at the upper left portion of the figure. (**A**) Examples of focal discharges. When two different discharges were present, they were independently illustrated. The left column corresponds to the left discharge, and the right column corresponds to the right discharge. (**B**) Examples of the generalized discharges. (**C**) Discharges submitted to source analyses with sLORETA in a different time window. (**D**) sLORETA solutions map showing the current densities according to their Brodmann's areas. (**E**) sLORETA solutions in a anatomical template (superior panel) and in a 3D rendering (middle panel). When there were two different discharges, the left discharge is depicted in the pink scale, and the right discharge is depicted in the jet or cold scale in (D) and (E). The inferior panel shows the VBM analysis results. The VBM results (colored areas) are superimposed on an anatomical template. The colors represent the number of standard deviations compared with the controls, as indicated by the scale in the right inferior portion of the figure. Green scale was used for abnormalities in the left (L) hemisphere and hot scale for abnormalities in the right (R) hemisphere. Patient 4 (see Fig. 1) had predominantly areas of atrophy and patient 14 (see Fig. 2) had areas of increased gray matter volumes. Statistical analysis was performed with a corrected $P < 0.05$ (false discovery rate). Figures are depicted in the neurological convention (right on right).

No previous studies have combined quantitative techniques, such as sLORETA and VBM analysis, to evaluate IGE patients. The concordance between these methods demonstrates that focal cortical abnormalities are present in some IGE patients. The pathophysiology of absence and myoclonic seizures are mainly related to the thalamocortical circuitry, and the findings described here reflect the involvement of the cortex in the mechanism behind these seizures in this group of patients. According to experimental studies, myoclonic and especially absence seizures may have a focal onset in the cortex [Avanzini et al., 2000; Meeren et al., 2002]. The discharge rapidly spreads to involve the thalamus. The interaction between the thalamus and cortex may be responsible for the maintenance of the seizure [Meeren et al., 2002].

Using quantitative EEG source analysis, a previous study investigated 25 absence seizures in five subjects [Holmes et al., 2004]. The authors observed that absence seizures likely involved selective cortical networks, including the orbital frontal and mesial frontal regions, which supported earlier findings [Meeren et al., 2002]. Our EEG quantitative evaluation was performed in interictal discharges but is inline with this investigation, showing clear focal discharges localized mainly in the frontal lobes (11 of 17 patients, 65%). This predominance may be responsible for the frontal lobe abnormalities observed in IGE patients in previous neuroimaging investigations of IGE [Betting et al., 2006a; Woermann et al., 1999].

Visual inspection of MRI scans showed that there were mild abnormalities in IGE patients [Betting et al., 2006b]. Using a standardized protocol for investigating epilepsy, we studied the MRI scans of 134 IGE patients. Of these patients, 33 (24%) showed abnormalities, most of which were nonspecific, including arachnoid cysts, cortical atrophy and signal alterations [Betting et al., 2006b]. In our current investigation, patients with abnormal MRI scans after visual analysis were excluded. The subtle and heterogeneous gray matter abnormalities that we detected in here may be associated with the minor abnormalities described previously.

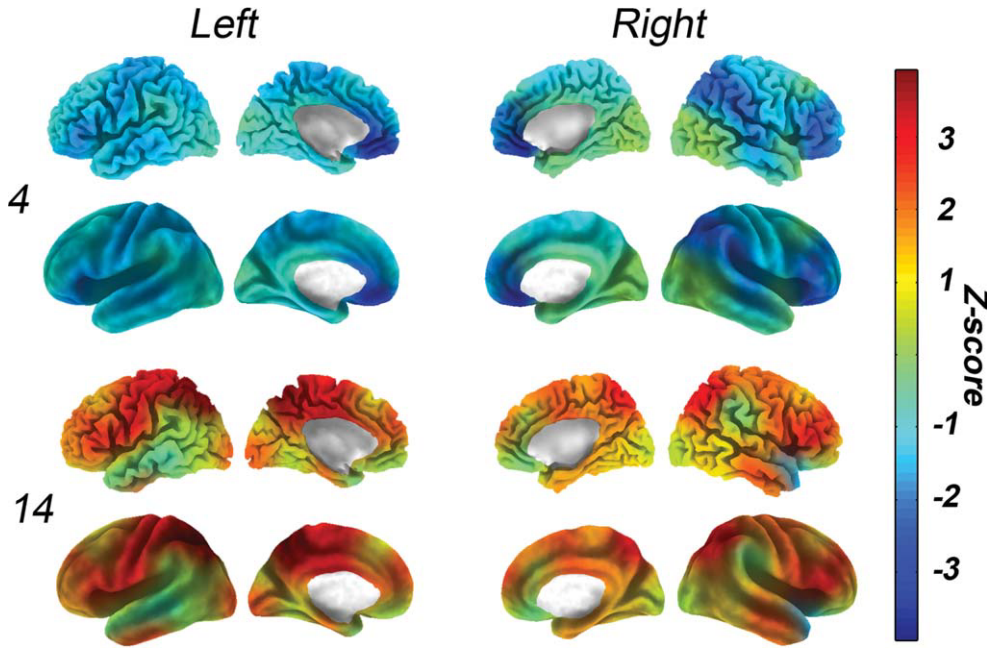

Figure 3.

ROI volumetry maps of patients 4 and 14. The volumes are standardized based on the normalized volumes of the control group (*Z*-score). Each color corresponds to the number of standard deviations compared with controls, as indicated by the colorbar. Hot colors correspond to areas of increased volumes, and cold colors correspond to decreased volumes compared with the controls. The superior panel shows an anatomical rendering and the inferior panel shows an inflated rendering. Patient number is displayed on the left. See the online Supporting Information for the volumetry maps from the rest of the patients.

Quantitative MRI investigations in IGE patients have provided several results. A study using VBM-individual analysis showed that 25% (five of 20) of JME patients had areas of gray matter abnormalities. Three patients showed areas with decreased gray matter volumes, and two patients had areas with increased gray matter volumes. The group comparison showed increased gray matter volumes localized in the frontal lobes [Woermann et al., 1999]. Our previous VBM-group analysis revealed increased gray matter areas in the frontal basal and mesiofrontal regions [Betting et al., 2006a]. Investigations of the brain using VBM in IGE patients showed increased gray matter volumes in the bilateral superior mesiofrontal regions, as well as decreased gray matter concentration in the prefrontal region and in other structures, including the cerebellum, and the frontal, parietal and temporal cortex [Ciumas and Savic, 2006; Kim et al., 2007; Tae et al., 2006]. Increased gray matter was also detected in the thalamus using VBM [Betting et al., 2006a]. Decreased thalamic volumes were also reported in patients with IGE [Chan et al., 2006; Ciumas and Savic, 2006; Helms et al., 2006]. Thalamic atrophy was correlated with the duration of the epilepsy in JME patients [Kim et al., 2007]. Additionally, other morphological abnormalities have been reported such as flattening of the brain in the craniocaudal direction in GTCS patients, reduced cortical thickness at the frontal and temporal lobes which was correlated with disease duration in JME patients and smaller subcortical volumes which were mainly characterized by putaminal atrophy in various IGE subsyndromes [Savic et al., 1998; Seeck et al., 2005; Tae et al., 2008]. These apparently conflicting findings parallel the heterogeneity observed in IGE patients. Our investigation also demonstrates this variability. For example, patients number 4 and 22 have similar ages and dramatically different GSW discharges in their EEGs. VBM showed diffuse areas of increased gray matter volumes in the frontal cortex, in the thalamus, caudate nucleus and basal ganglia. The volumetry profiles also showed divergent patterns, with patient 4 having predominant areas of atrophy and patient 22 showing areas of increased volumes in comparison to the controls. Moreover, some of the patients we studied did not present abnormalities in VBM analysis, indicating that another major mechanism caused the disease in these individuals. In addition to the variations between the EEG results and structural findings in IGE patients, there is significant variability in the clinical observations between patients. The spatial diversity of the gray matter abnormalities and the absence of a pattern for each IGE subsyndrome also emphasize the heterogeneity and may be related with the clinical variability

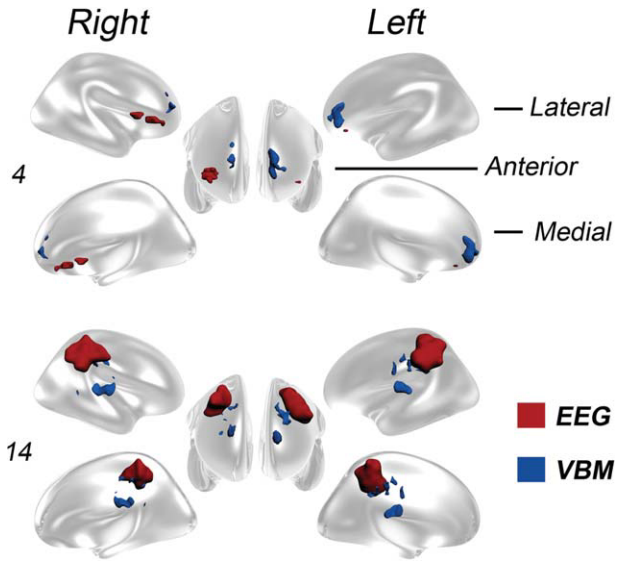

Figure 4.

Three-dimensional render of the brain overlaid with a graphical representation of the region with highest current density detected by sLORETA and the clusters of VBM statistically significant voxels. EEG source detection results are displayed in red and VBM in blue colors. The renders of two patients (4 and 14) are shown in lateral, anterior and medial views of the right and left hemispheres. See the online Supporting Information for the render from the rest of the patients.

observed in these patients. Genetic predisposition and environmental factors can influence the brain, and these variables influence the final phenotype of each IGE patient. The complex profiles are confirmed by genetic studies, which showed that most IGE cases have a polygenic basis. Only a few IGE patients were shown to be due to a monogenic disorder caused by abnormal neuronal GABA receptors or ion channels [Helbig et al., 2008].

The use of individual VBM analysis may have drawbacks. There is an increased rate of false positives results especially characterized by gray matter reduction [Salmond et al., 2002]. Furthermore, previous investigations using VBM for the evaluation of individual patients with normal MRI were unable to detect abnormalities [Eriksson et al., 2009; Salmenpera et al., 2007]. The authors concluded that this methodology may not be suitable to detect occult abnormalities possibly associated with seizure onset zone in individual patients with unremarkable standard structural MRI. However, in some cases quantitative MRI may be useful [Salmenpera et al., 2007]. This problem may be secondary to methodological issues, specially normalization and statistical significance thresholding [Eriksson et al., 2009]. Individual VBM analysis is less sensitive to areas of great variability like the mesial temporal lobes and areas of decreased gray matter. Despite of these limitations, studies using individual VBM analysis in patients with focal cortical dysplasia showed that this method is able to detect gray matter abnormalities in a majority of patients and the abnormal areas extend beyond the visible lesion [Bonilha et al., 2006; Colliot et al., 2006]. The patients investigated in here had predominantly neocortical and areas of increased gray matter volumes. The use of VBM comparisons in the control group, the use of two distinct methods for source analysis and ROI volumetry also strengthened the findings of our study. The pattern of structural abnormality observed here is in accordance with previous findings and to the hypothesized pathophysiology of IGE.

The abnormal cortical areas detected by morphometric analyses may correspond to structural defects, such as dysplasia, which would be in agreement with previous descriptions of histopathological abnormalities in patients with JME [Meencke and Janz, 1984]. Additionally, this hypothesis is also reinforced by the predominance of cases with increased gray matter in our investigation (88% of the patients with abnormalities, as detected by VBM) and in previous studies using VBM-group analysis [Betting et al., 2006; Kim et al., 2007; Woermann et al., 1999]. Another feasible explanation for the abnormalities detected by VBM analysis is that these areas may represent changes in neuronal connectivity [Woermann et al., 1999]. Neuronal connectivity changes can be closely related to neuronal function and have been measured with MRS via reduced concentrations of N-acetylaspartate [Savic et al., 2000; Simister et al., 2003].

Focal epilepsies occasionally show generalized discharges in EEG recordings as a result of a secondary bisynchrony [Tükel and Jasper, 1952]. Furthermore, auras are commonly reported in patients with generalized epilepsies [Boylan et al., 2006]. These peculiarities can lead to an erroneous epilepsy syndrome diagnosis. In these situations, the exact classification of patients may be difficult, and it is important to be mindful that the EEG and MRI results may reveal intermediary clinical situations. Basically, classifications try to group common diseases in order to facilitate the clinical practice, teaching and research. It must be remembered that, in some cases as presented here, the whole clinical, EEG and MRI picture may reveal intermediary situations.

ACKNOWLEDGMENTS

The authors and their immediate family members have no competing financial interests related to this article.

REFERENCES

Aléman-Gómez Y, Melie-García L, Valdés-Hernandez P. BASPM: Toolbox for automatic parcellation of brain structures [CD]. Proceedings of the 12th Annual Meeting of the Organization for Human Brain Mapping; 2006 June 11–15; Florence, Italy. Neuroimage 27, 2006.

Ashburner J, Friston KJ (2005): Unified segmentation. Neuroimage 26:839–851.

Avanzini G, Binelli S, Franceschetti S, Panzica F, Pozzi A (2000): Pathophysiology of myoclonus in Janz syndrome. In: Schmitz B, Sander T, editors. Juvenile Myoclonic Epilepsy: The Janz

Syndrome. Petersfield, UK: Wrightson Biomedical Publishing. pp 57–72.
Bagshaw A, Kobayashi E, Dubeau F, Pike G, Gotman J (2005): Correspondence between EEG-fMRI and EEG dipole localisation of interictal discharges in focal epilepsy. Neuroimage 30:417–425.
Betting LE, Mory SB, Lopes-Cendes I, Li LM, Guerreiro MM, Guerreiro CAM, Cendes F (2006a): Voxel-based morphometry in patients with idiopathic generalizes epilepsies. Neuroimage 32:498–502.
Betting LE, Mory SB, Lopes-Cendes I, Li LM, Guerreiro MM, Guerreiro CAM, Cendes F (2006b): MRI reveals structural abnormalities in patients with idiopathic generalized epilepsy. Neurology 67:848–852.
Bonilha L, Montenegro MA, Rorden C, Castellano G, Guerreiro MM, Cendes F, Li LM (2006): Voxel-based morphometry reveals excess gray matter concentration in patients with focal cortical dysplasia. Epilepsia 47:908–915.
Boylan LS, Labovitz DL, Jackson SC, Starner K, Devinsky O (2006): Auras are frequent in idiopathic generalized epilepsy. Neurology 67:343–345.
Chan CH, Briellmann RS, Pell GS, Scheffer IE, Abbott DF, Jackson GD (2006): Thalamic atrophy in childhood absence epilepsy. Epilepsia 47:399–405.
Ciumas C, Savic I (2006): Structural changes in patients with primary generalized tonic and clonic seizures. Neurology 67:683–686.
Colliot O, Bernasconi N, Khalili N, Antel SB, Naessens V, Bernasconi A (2006): Individual voxel-based analysis of gray matter in focal cortical dysplasia. Neuroimage 29:162–171.
Commission on Classification and Terminology of the International League Against Epilepsy (1989): Proposal for revised classification of epilepsies and epileptic syndromes. Epilepsia 30:389–399.
Eriksson SH, Thom M, Symms MR, Focke NK, Martinian L, Sisodiya SM, Duncan JS (2009): Cortical neuronal loss and hippocampal sclerosis are not detected by voxel-based morphometry in individual epilepsy surgery patients. Hum Brain Mapp 30:3351–3360.
Gloor P (1968): Generalized cortico-reticular epilepsies: Some considerations on the pathophysiology of generalized bilaterally synchronous spike and wave discharge. Epilepsia 9:249–263.
Grova C, Daunizeau J, Kobayashi E, Bagshaw AP, Lina J-M. Dubeau F, Gotman J (2008): Concordance between distributed EEG source localization and simultaneous EEG-fMRI studies of epileptic spikes. Neuroimage 39:755–774
Grova C, Daunizeau J, Lina JM, Bénar CG, Benali H, Gotman J (2006): Evaluation of EEG localization methods using realistic simulations of interictal spikes. Neuroimage 29:734–753.
Helbig I, Scheffer IE, Mulley JC, Berkovic SF (2008): Navigating the channels and beyond: Unraveling the genetics of the epilepsies. Lancet Neurol 7:231–245.
Helms G, Ciumas C, Kyaga S, Savic I (2006): Increased thalamus levels of glutamate and glutamine (Glx) in patients with idiopathic generalized epilepsy. J Neurol Neurosurg Psychiatry 77:489–494.
Holmes MD, Brown M, Tucker DM (2004): Are "generalized" seizures truly generalized? Evidence of localized mesial frontal and frontopolar discharges in absence. Epilepsia 45:1568–1579.
Huppertz HJ, Hoegg S, Sick C, Lücking CH, Zentner J, Schulze-Bonhage A, Kristeva-Feige R (2001): Cortical current density reconstruction of interictal epileptiform activity in temporal lobe epilepsy. Clin Neurophysiol 112:1761–1772.
Kim JH, Lee JK, Koh SB, Lee SA, Lee JM, Kim SI, Kang JK (2007): Regional grey matter abnormalities in juvenile myoclonic epilepsy: A voxel-based morphometry study. Neuroimage 37:1132–1137.
Koepp MJ, Woermann FG (2005): Imaging structure and function in refractory focal epilepsy. Lancet Neurol 4:42–53.
Lombroso CT (1997): Consistent EEG focalities detected in subjects with primary generalized epilepsies monitored for two decades. Epilepsia 38:797–812.
Meencke HJ, Janz D (1984): Neuropathological findings in primary generalized epilepsy: A study of eight cases. Epilepsia 25: 8–21.
Meeren HK, Pijn JP, Van Luijtelaar EL, Coenen AM, Lopes da Silva FH (2002): Cortical focus drives widespread corticothalamic networks during spontaneous absence seizures in rats. J Neurosci 22:1480–1495.
Meisenzahl EM, Koutsouleris N, Gaser C, Bottlender R, Schmitt GJ, McGuire P, Decker P, Burgermeister B, Born C, Reiser M, Möller HJ (2008): Structural brain alterations in subjects at high-risk of psychosis: A voxel-based morphometric study. Schizophr Res 102:150–162.
Mulert C, Jäger L, Schmitt R, Bussfeld P, Pogarell O, Möller H, Juckel G, Hegerl U (2004): Integration of fMRI and simultaneous EEG: Towards a comprehensive understanding of localization and timecourse of brain activity in target detection. Neuroimage 22:83–94.
Panayiotopoulos CP (2002): Idiopathic generalized epilepsies. In: Panayiotopoulos CP, editor. A Clinical Guide to Epileptic Syndromes and Their Treatment. Oxfordshire, UK: Bladon Medical Publishing. pp 115–160.
Pascual-Marqui RD (2002): Standardized low-resolution brain electromagnetic tomography (sLORETA): Technical details. Methods Find Exp Clin Pharmacol 24 (suppl D):5–12.
Rorden C, Brett M (2000). Stereotaxic display of brain lesions. Behav Neurol 12:191–200.
Salmenpera TM, Symms MR, Rugg-Gunn FJ, Boulby PA, Free SL, Barker GJ, Yousry TA, Duncan JS (2007): Evaluation of quantitative magnetic resonance imaging contrasts in MRI-negative refractory focal epilepsy. Epilepsia 48:229–237.
Salmond CH, Ashburner J, Vargha-Khadem F, Connelly A, Gadian DG, Friston KJ (2002): Distributional assumptions in voxel-based morphometry. Neuroimage 17:1027–1030.
Savic I, Lekvall A, Greitz D, Helms G (2000): MR spectroscopy shows reduced frontal lobe concentrations of *n*-acetyl aspartate in patients with juvenile myoclonic epilepsy. Epilepsia 41:290–296.
Savic I, Seitz RJ, Pauli S (1998): Brain distortions in patients with primary generalized tonic-clonic seizures. Epilepsia 39:364–370.
Scherg M, Bast T, Berg P (1999): Multiple source analysis of interictal spikes: Goals, requirements, and clinical value. J Clin Neurophysiol 16:214–224.
Seeck M, Dreifuss S, Lantz G, Jallon P, Foletti G, Despland PA, Delavelle J, Lazeyras F (2005): Subcortical nuclei volumetry in idiopathic generalized epilepsy. Epilepsia 46:1642–1645.
Simister RJ, McLean MA, Barker GJ, Duncan JS (2003): Proton MRS reveals frontal lobe metabolite abnormalities in idiopathic generalized epilepsy. Neurology 61:897–902.
Tae WS, Hong SB, Joo EY, Han SJ, Cho JW, Seo DW, Lee JM, Kim IY, Byun HS, Kim SI (2006): Structural brain abnormalities in juvenile myoclonic epilepsy patients: Volumetry and voxel-based morphometry. Korean J Radiol 7:162–172.

Tae WS, Kim SH, Joo EY, Han SJ, Kim IY, Kim SI, Lee JM, Hong SB (2008): Cortical thickness abnormality in juvenile myoclonic epilepsy. J Neurol 255:561–566.

Talairach J, Tournoux P (1988): Co-planar stereotaxic atlas of the human brain. Stuttgart: Thieme.

Tükel K, Jasper H (1952): The electroencephalogram in parasagittal lesions. Electroencephalogr Clin Neurophysiol 4:481–494.

Waltz S (2000): The EEG in juvenile myoclonic epilepsy. In: Schmitz B, Sander T, editors. Juvenile myoclonic epilepsy: The Janz syndrome. Petersfield (UK): Wrightson Biomedical Publishing. pp 41–55.

Woermann FG, Free SL, Koepp MJ, Sisodiya SM, Duncan JS (1999): Abnormal cerebral structure in juvenile myoclonic epilepsy demonstrated with voxel-based analysis of MRI. Brain 122:2101–2108.

Zumsteg D, Friedman A, Wieser HG, Wennberg RA (2006). Source localization of interictal epileptiform discharges: Comparison of three different techniques to improve signal to noise ratio. Clin Neurophysiol 117:562–571.